JACS
JOURNAL OF THE AMERICAN CHEMICAL SOCIETY
Article
pubs.acs.org/JACS

Theoretical Elucidation of the Origins of Substituent and Strain Effects on the Rates of Diels–Alder Reactions of 1,2,4,5-Tetrazines

Fang Liu, Yong Liang, and K. N. Houk*

Department of Chemistry and Biochemistry, University of California, Los Angeles, California 90095, United States

Supporting Information

ABSTRACT: The Diels–Alder reactions of seven 1,2,4,5-tetrazines with unstrained and strained alkenes and alkynes were studied with quantum mechanical calculations (M06-2X density functional theory) and analyzed with the distortion/interaction model. The higher reactivities of alkenes compared to alkynes in the Diels–Alder reactions with tetrazines arise from the differences in both interaction and distortion energies. Alkenes have HOMO energies higher than those of alkynes and therefore stronger interaction energies in inverse-electron-demand Diels–Alder reactions with tetrazines. We have also found that the energies to distort alkenes into the Diels–Alder transition-state geometries are smaller than for alkynes in these reactions. The strained dienophiles, *trans*-cyclooctene and cyclooctyne, are much more reactive than unstrained *trans*-2-butene and 2-butyne, because they are predistorted toward the Diels–Alder transition structures. The reactivities of substituted tetrazines correlate with the electron-withdrawing abilities of the substituents. Electron-withdrawing groups lower the LUMO+1 of tetrazines, resulting in stronger interactions with the HOMO of dienophiles. Moreover, electron-withdrawing substituents destabilize the tetrazines, and this leads to smaller distortion energies in the Diels–Alder transition states.

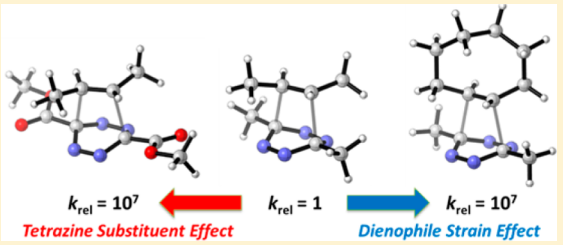

INTRODUCTION

Tetrazine cycloadditions have received increased attention in bioorthogonal chemistry[1] since the application of inverse-electron-demand Diels–Alder reactions of 1,2,4,5-tetrazines and strained alkenes in 2008.[2] In these pioneering studies, *trans*-cyclooctene and norbornene were found to undergo rapid reactions as dienophiles in Diels–Alder reactions. The *trans*-cyclooctene–tetrazine cycloaddition (Figure 1) has an extremely high second-order rate constant of up to 10^4 M^{-1} s^{-1}, and this reaction has been widely used in bioimaging.[3] Later, cyclopropenes,[4] cyclobutene derivatives,[5] and cyclooctynes[6] were explored as dienophiles with tetrazines, adding an extra dimension to strain-promoted, or as we have identified, distortion-accelerated,[7] cycloadditions in bioorthogonal chemistry.

Figure 1. Bioorthogonal *trans*-cyclooctene–tetrazine cycloaddition.

Tetrazine cycloadditions are not limited to bioorthogonal chemistry. These cycloaddition reactions have also been used in synthesis of natural products,[8] modification of metal–organic frameworks,[9] functionalization of carbon nanotubes,[10] and construction of microarrays.[11] In fact, the Diels–Alder reactions of tetrazines are venerable processes that have been studied in detail by the Sauer group[12] and others[13] in the past half century. Sauer and co-workers reported kinetic measurements of cycloaddition reactions of tetrazines with a series of dienophiles. Along with a more comprehensive exploration of substituents, these studies identified significant differences in rate constants between strained and unstrained alkenes and alkynes.[12c]

Scheme 1 shows the second-order rate constants measured experimentally by Sauer et al. for the cycloaddition reactions between dimethyl 1,2,4,5-tetrazine-3,6-dicarboxylate and acetylene, ethylene, *trans*-4-octene, cyclooctyne, and *trans*-cyclooctene.[12c] The rate constants measured with strained dienophiles (cyclooctyne and *trans*-cyclooctene) are about 5 orders of magnitude greater than those of unstrained parent dienophiles (acetylene and ethylene). For *trans*-cyclooctene and *trans*-4-octene, which have the same substituent pattern, the rate constant difference is nearly 7 orders of magnitude! In addition, the reactions of alkenes with tetrazine are about 1000 times faster than alkynes. The origins of such striking differences have not been explored previously.

The much higher reactivity of strained dienophiles is usually attributed to the strain-release after the cycloaddition. However, the strain-release theory would predict the opposite reactivity difference between *trans*-cyclooctene and cyclooctyne. As shown in Scheme 2, the strain-release from *trans*-cyclooctene to cyclooctane is 7.4 kcal/mol less than that from cyclooctyne to *cis*-cyclooctene,[14] but *trans*-cyclooctene reacts 2–3 orders of magnitude faster than cyclooctyne in the tetrazine cyclo-

Received: June 3, 2014
Published: July 19, 2014

   dx.doi.org/10.1021/ja505569a | J. Am. Chem. Soc. 2014, 136, 11483–11493

Scheme 1. Rate Constants of the Tetrazine Diels–Alder Reactions with Strained and Unstrained Alkenes and Alkynes

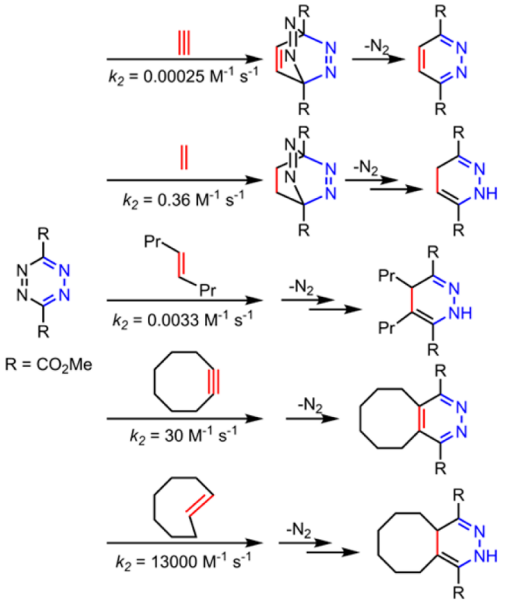

Scheme 2. Strain Energies (SE, in kcal/mol) in *trans*-Cyclooctene, Cyclooctyne, and the Reduced Compounds

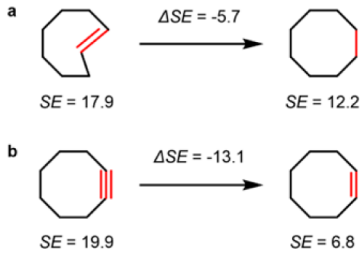

additions (Scheme 1). We have undertaken a theoretical investigation of the Diels–Alder reactivities of strained and unstrained alkenes and alkynes and report here the origins of these reactivity differences.

There have been many experimental studies of substituent effects on reactivities of tetrazines. Hilderbrand and co-workers reported reaction rates for a series of 1,2,4,5-tetrazines in cycloaddition reactions with *trans*-cyclooctenol, which has been used for bioorthogonal conjugations.[15] Their study showed that methyl-substituted tetrazine is less reactive than pyridyl- or pyrimidyl-substituted tetrazine (Scheme 3a). The studies of reactions of substituted tetrazines with cyclooctyne showed that dipyridyltetrazine is more reactive than diphenyltetrazine (Scheme 3b).[6a] Tetrazines substituted with electron-donor groups are the least reactive species in the tetrazine family. Scheme 3c shows a comparison between the parent tetrazine, 3,6-diphenyltetrazine, and 3-methoxy-6-methylthio-1,2,4,5-tetrazine. Tetrazine itself reacts with phenylacetylene at 70 °C;[12e] the reaction of diphenyltetrazine requires higher temperature of 110 °C,[13a] while the reaction between 3-methoxy-6-methylthio-1,2,4,5-tetrazine and phenylacetylene occurs at 180 °C.[13c]

Tetrazines are known to undergo inverse-electron-demand Diels–Alder reactions with alkenes or alkynes. Figure 2 shows the π orbitals of acetylene (left), the parent tetrazine (middle), and ethylene (right). Because tetrazine is an electron-deficient diene with low-lying vacant orbitals, the interaction between

Scheme 3. Substituent Effects on the Diels–Alder Reactivities of Tetrazines

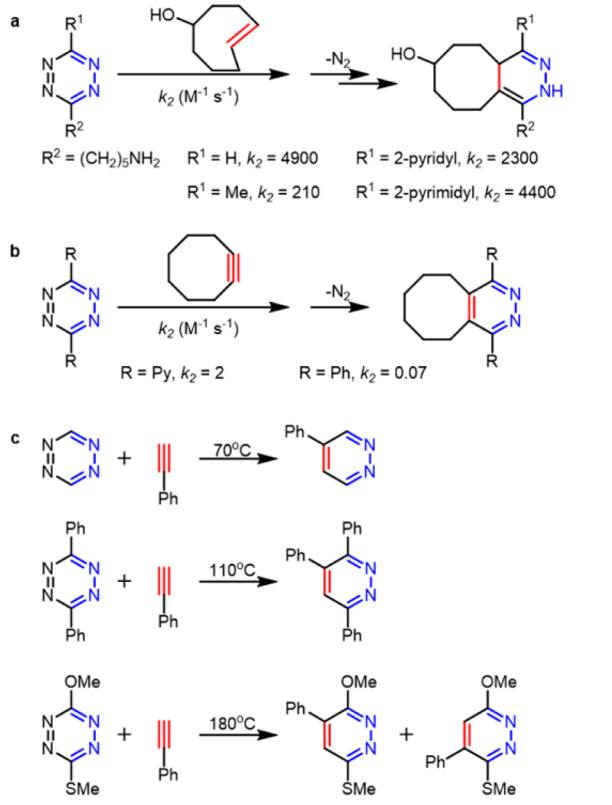

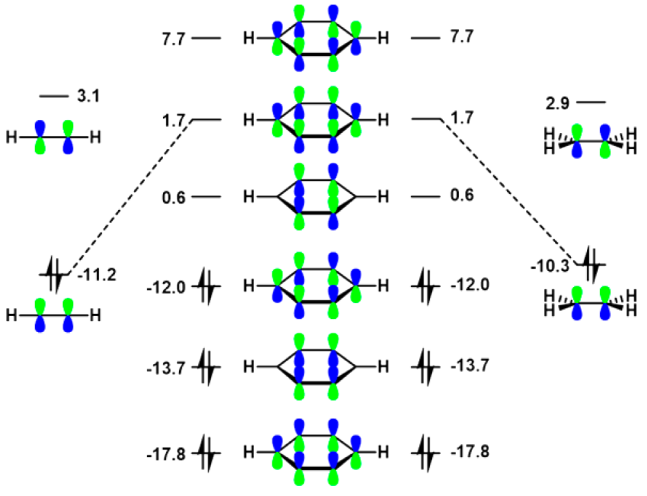

Figure 2. π Orbitals of acetylene, parent tetrazine, and ethylene. The orbital energies (in eV) are computed with HF/6-311+G(d,p), and the HOMO–LUMO+1 interactions between tetrazine and acetylene or ethylene are indicated by dashed lines.

the LUMO+1 (the π^* orbital that interacts with the dienophile HOMO in the Diels–Alder reaction) of tetrazine and HOMO of acetylene or ethylene is a key factor that influences the reactivity of the Diels–Alder reaction. The LUMO+1 energy of tetrazine is further lowered by an electron-withdrawing substituent, resulting in a decrease in HOMO–LUMO+1 gap, and an increase in reactivity. On the contrary, electron-donating groups raise LUMO+1 and reduce the reactivity of tetrazine.

dx.doi.org/10.1021/ja505569a | J. Am. Chem. Soc. 2014, 136, 11483–11493

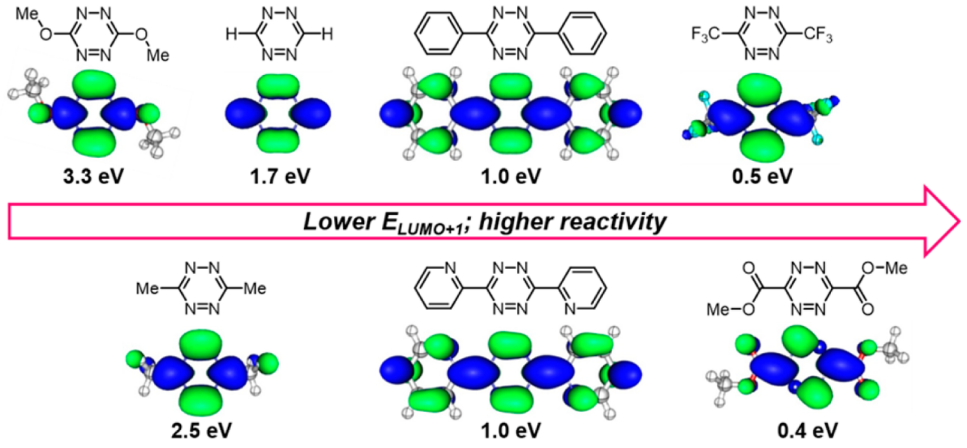

Figure 3. Low-lying vacant orbitals of tetrazines involved in the Diels–Alder reaction. HF/6-311+G(d,p) energies of these orbitals are shown below the orbitals.

LUMO+1 orbital energies were calculated with HF/6-311+G(d,p) for a series of tetrazines. The LUMO+1 orbital shapes and energies are shown in Figure 3. The lowering of LUMO+1 results in greater reactivity, although diphenyltetrazine is about 30 times less reactive than dipyridyltetrazine (Scheme 3b), despite the same energy of LUMO+1 orbitals of the two, and parent tetrazine has higher LUMO+1 orbital energy but is more reactive than diphenyltetrazine (Scheme 3c).

To better understand these data, we have undertaken a comprehensive investigation of the substituent and strain effects on the rates of Diels–Alder reactions of tetrazines with a variety of alkenes and alkynes using density functional theory (DFT) calculations. We provide a detailed analysis of the controlling factors for the Diels–Alder reactivity using the distortion/interaction model. We have studied the cycloaddition reactions of the dienes and dienophiles shown in Figure 4: the electron-donor-substituted tetrazines **1** and **2**,

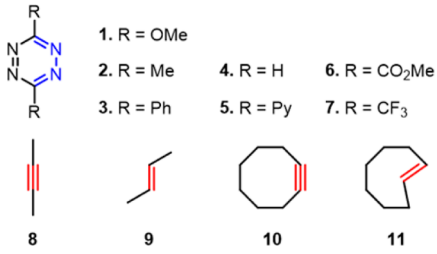

Figure 4. Tetrazines and dienophiles investigated.

conjugating-group-substituted tetrazines **3** and **5**, the parent tetrazine **4**, and electron-acceptor-substituted tetrazines **5**–**7**. The dienophiles studied are strained and unstrained alkenes and alkynes, including 2-butyne **8**, *trans*-2-butene **9**, cyclooctyne **10**, and *trans*-cyclooctene **11**.

COMPUTATIONAL METHODS

The DFT calculations were performed with Gaussian 09.[16] Geometry optimizations of all the minima and transition states were carried out at the M06-2X level of theory with the 6-31G(d) basis set.[17] Vibrational frequencies were computed at the same level to verify that optimized structures are energy minima or transition states and to evaluate zero-point vibrational energies (ZPVE) and thermal corrections at 298 K. A quasiharmonic correction was applied during the entropy calculation by setting all positive frequencies that are less than 100 cm^{-1} to 100 cm^{-1}.[18] This method has been found to give relatively accurate energetics for cycloadditions.[19] We also tested the energetics of reactions with a larger basis set, 6-311+G(d,p). This caused a systematic increase in activation energy by 0.5–1.0 kcal/mol. Because of the considerably greater cost of these calculations, and the lack of significant change in results, we have used the smaller basis set for the data reported here for the 28 reactions studied.

Solvent effects in 1,4-dioxane were computed at the M06-2X/6-311+G(d,p) level using the gas-phase optimized structures for the Diels–Alder reactions of 3,6-bis(trifluoromethyl)tetrazine. Solvation energies were evaluated by a self-consistent reaction field (SCRF) using the CPCM model,[20] where UFF radii were used. Figure 5 shows

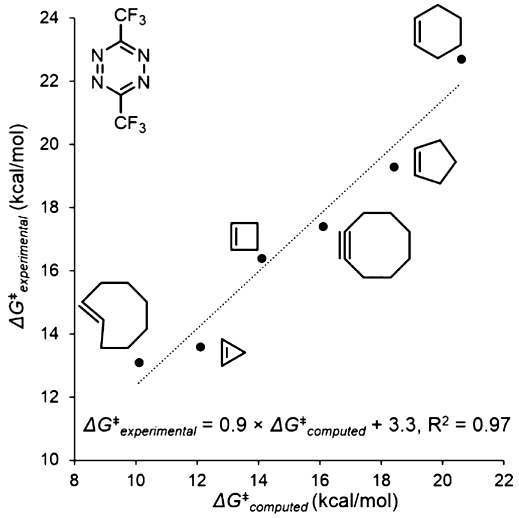

Figure 5. Correlation between computed activation free energies in 1,4-dioxane and those derived from experimental rate constants.

the correlation between these computed activation free energies and those obtained from experimental rate constants.[12c] The correlation is very good but with a systematic deviation of 3.3 kcal/mol.

The frontier molecular orbitals (FMOs) and their energies were computed at the HF/6-311+G(d,p) level using the M06-2X/6-31G(d) geometries. This is because Kohn–Sham orbitals often provide poor estimates of ionization potentials of simple organic molecules, and the medium size 6-31G(d) basis set often gives inaccurate unoccupied orbital eigenvalues.[21] Distortion and interaction energies, as well as intrinsic reaction coordinates (IRCs) were carried out at the M06-2X/6-31G(d) level. Constrained optimizations with designated distortion angles of tetrazines **1**–**7** and dienophiles **8** and **9** were performed with M06-2X/6-31G(d).

dx.doi.org/10.1021/ja505569a | J. Am. Chem. Soc. 2014, 136, 11483–11493

RESULTS AND DISCUSSION

Influence of Dienophile Strain and Distortion Energies on the Diels–Alder Reactivity. The transition structures for the Diels–Alder reactions between tetrazine **2** and dienophiles **8**–**11** are shown in Figure 6. The forming

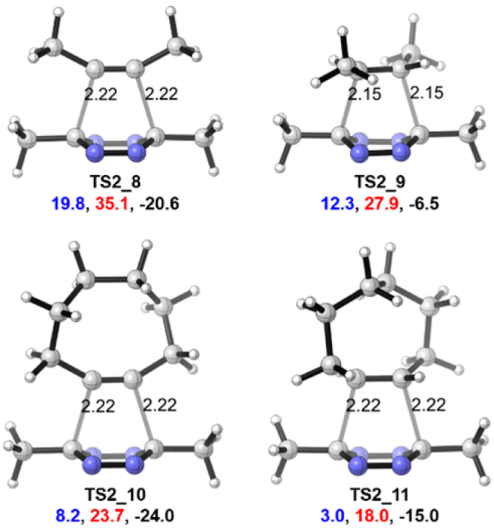

Figure 6. M06-2*X*/6-31G(d)-optimized transition structures for reactions of 3,6-dimethyltetrazine **2** with 2-butyne **8**, *trans*-2-butene **9**, cyclooctyne **10**, and *trans*-cyclooctene **11** (forming C–C bond distances are labeled in Å; $\Delta H^{\ddagger}$, $\Delta G^{\ddagger}$, and ΔG_{rxn} are shown below each structure in kcal/mol in blue, red, and black, respectively).

bond lengths are shown in angstroms. The activation enthalpy ($\Delta H^{\ddagger}$), activation free energy ($\Delta G^{\ddagger}$), and reaction free energy (ΔG_{rxn}) for each combination are shown below each structure in kcal/mol in blue, red, and black, respectively. The transition structures for the Diels–Alder reactions between the other six tetrazines and dienophiles **8**-**11** are provided in the Supporting Information (SI).

The activation free energy for the reaction of 3,6-dimethyltetrazine with *trans*-2-butene **9** is 9.9 kcal/mol higher than that with strained *trans*-cyclooctene **11** (Figure 6, **TS2_9** and **TS2_11**), which corresponds to 7 orders of magnitude difference between rate constants. This is consistent with the experimental observations on related compounds (Scheme 1).[22] Similarly, the difference in calculated activation free energies for reactions of 3,6-dimethyltetrazine with 2-butyne **8** and strained cyclooctyne **10** is 11.4 kcal/mol (Figure 6, **TS2_8** and **TS2_10**), leading to a predicted rate difference of 10^8.

Figure 7 summarizes the activation free energies of all 28 reactions studied here. The boxes in the figure are color coded. As the colors change from green to yellow and to red, the activation free energies increase. The corresponding second-order rate constants at 298 K computed from Eyring transition state theory are listed on the right of the color bar. The figure is arranged in order of increasing reactivity of the tetrazines, from left to right. The dienophiles are also ranked in order of reactivity, increasing from top to bottom. The range of reactivities is enormous, with activation free energies ranging from 8 to 35 kcal/mol, corresponding to a 10^{20} range in rate constants at room temperature!

After the submission of this paper, Kuntner, Mikula, and co-workers reported rate constants for the reactions of 3-(3-fluoropropyl)-6-methyltetrazine with *trans*-cyclooctenes and the uses of these reactions in ^{18}F PET imaging.[3k] The measured activation free energy of 17.5 kcal/mol from their work is very close to our prediction of 18.0 kcal/mol in Figure 7. The measured rate constant of 1.5 M^{-1} s^{-1} in 1,4-dioxane is similar to that predicted from TS theory, although here we are neglecting solvation energetics and slight variations in temperature. These predictions overestimate somewhat the rates of reactions of the most reactive tetrazines and dienophiles but in general are within an order of magnitude of the solution rates in dioxane or other organic solvents. This should provide a useful guide to experimentalists about the rates of reactions not yet explored experimentally.

Because of the enormous rate variations, these reactions can be used for many different purposes. The very slow reactions, labeled in red, can still be achieved at elevated temperatures, and these reactants are quite stable. The reactions marked in yellow occur only slowly under concentrated conditions at room temperature but are in the range of rates typical for synthetically useful reactions. The light green coded reactions occur rapidly at room temperature, and some of them have been used for detection of biomolecules in vitro even with low concentrations.[1f,g] The dark green labels indicate reactions that are very fast, useful for following cellular processes in vivo, but the highly reactive tetrazines **6** and **7** can also react with water and other biological nucleophiles.[2a,4f]

Our results and the experiments in Scheme 1 showed that alkenes, both unstrained and strained, are better dienophiles than alkyne counterparts in the Diels–Alder reactions with tetrazines; the differences in activation free energies are large, 4–10 kcal/mol for *trans*-2-butene/2-butyne and 3–6 kcal/mol for *trans*-cyclooctene/cyclooctyne (Figure 7; see the Supporting Information for activation enthalpies). This difference between alkene and alkyne is unexpected from our previous studies on the 1,3-dipolar cycloadditions of 24 1,3-dipoles, where ethylene and acetylene were predicted to have very similar reactivities with all 24 1,3-dipoles.[19b,23]

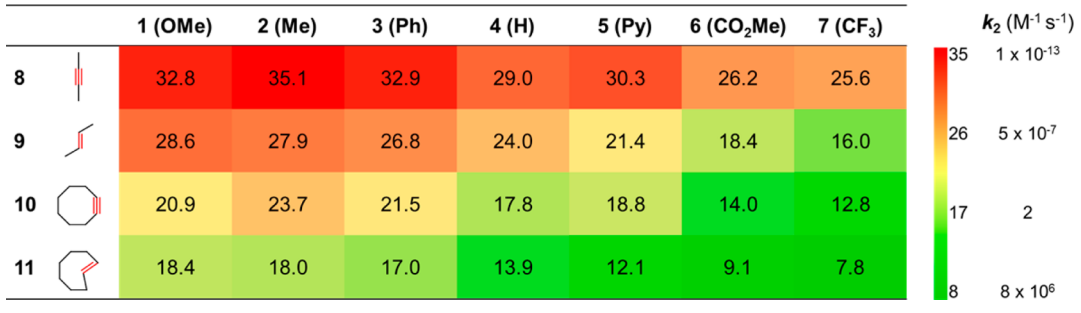

Figure 7. Reactivity map for the Diels–Alder reactions between tetrazines **1**–**7** and dienophiles **8**–**11** (activation free energies are in kcal/mol).

dx.doi.org/10.1021/ja505569a | J. Am. Chem. Soc. 2014, 136, 11483–11493

To understand why alkenes are more reactive than alkynes in the tetrazine Diels–Alder reactions, and why strained dienophiles are more reactive than unstrained species, distortion/interaction analyses[23−25] were performed on all transition states. The distortion/interaction model is illustrated in Figure 8 on the left, with the Diels–Alder reaction between

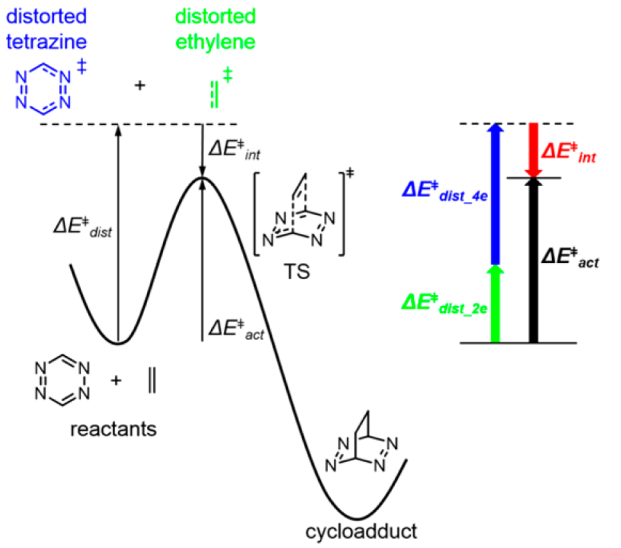

Figure 8. Distortion/interaction model.

parent tetrazine and ethylene as an example. The solid black curve in Figure 8 represents the potential energy along the reaction coordinate for the corresponding reaction. The transition structure is separated into two fragments (distorted tetrazine and distorted ethylene), followed by single-point energy calculations on each fragment. The energy difference between the distorted structures and optimized ground-state structures are the distortion energies of diene ($\Delta E^{\ddagger}_{dist\_4e}$) and dienophile ($\Delta E^{\ddagger}_{dist\_2e}$), respectively. The difference between the activation energy ($\Delta E^{\ddagger}_{act}$) and the total distortion energy ($\Delta E^{\ddagger}_{dist} = \Delta E^{\ddagger}_{dist\_4e} + \Delta E^{\ddagger}_{dist\_2e}$) is the interaction energy ($\Delta E^{\ddagger}_{int}$). The relationships between activation, distortion, and interaction energies are shown on the right of Figure 8.

The activation, distortion, and interaction energies for each transition structure involving dienophiles **8** and **9** are graphically displayed for each disubstituted tetrazine (labeled by the substituent groups) in Figure 9 on the left. Empty squares connected with dashed lines represent the Diels–Alder reactions with *trans*-2-butene **9**; the solid circles connected with solid lines are for reactions with 2-butyne **8**. The graph shows that the differences in reactivities between alkene and alkyne arise from differences in both distortion and interaction energies. The difference in interaction energies is expected based on FMO theory. Because the alkene has a HOMO energy higher than that of the alkyne (Figure 2), the HOMO–LUMO+1 gap between alkene and tetrazine is smaller, resulting in stronger interaction energy. The interaction energies along the series peak at the unsubstituted tetrazine (R = H) and increase with donors and acceptors. This trend can be attributed to the interplay between the effect of an increase in HOMO–LUMO+1 interaction, which becomes larger from left to right as the tetrazine becomes more electrophilic, and the shift from late TS to early TS along the series as the tetrazine becomes more reactive. In an earlier transition state, the interaction energy becomes smaller. We discuss this in more detail later.

The difference in distortion energies for alkene and alkyne reactions was, however, unexpected, because we expected an alkyne to be easier to distort than an alkene according to bending force constants.[26] To investigate this phenomenon, we performed constrained optimizations on *trans*-2-butene and 2-butyne, bending substituents (methyl groups or hydrogen atoms) out of planarity or linearity. This is the most significant distortion occurring in the Diels–Alder transition states involving alkenes or alkynes. For *trans*-2-butene, the distortion angle φ, the dihedral angle between the CH_3–C=C plane of the bent *trans*-2-butene and the original plane of the carbon skeleton of *trans*-2-butene (Figure 10), is gradually changed from 180° (as in ground-state structure) to 160°, in intervals of 2.5°. In the case of 2-butyne, the distortion angle θ, the angle between the bent bond and the triple bond (Figure 10), is gradually changed from 180° (as in ground-state structure) to 140°, in intervals of 5°. The energy difference between the optimized structure with fixed distortion angle and the ground-state structure is defined as the angular distortion energy ($\Delta E^{\ddagger}_{dist(\varphi)}$ or $\Delta E^{\ddagger}_{dist(\theta)}$). Figure 10 shows the plots of these energies versus distortion angles φ and θ. Distortion angles φ and θ range from 167° to 165° and 155° to 151° in transition

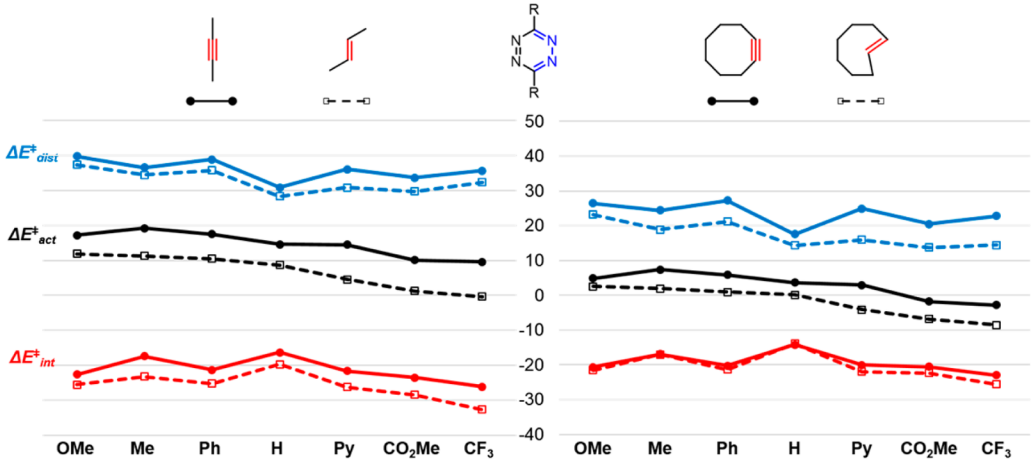

Figure 9. Plot of $\Delta E^{\ddagger}_{act}$ (black), $\Delta E^{\ddagger}_{dist}$ (blue), and $\Delta E^{\ddagger}_{int}$ (red) for tetrazines **1**–**7** in the Diels–Alder reactions with (left) *trans*-2-butene (dashed lines) and 2-butyne (solid lines) and (right) *trans*-cyclooctene (dashed lines) and cyclooctyne (solid lines).

dx.doi.org/10.1021/ja505569a | J. Am. Chem. Soc. 2014, 136, 11483−11493

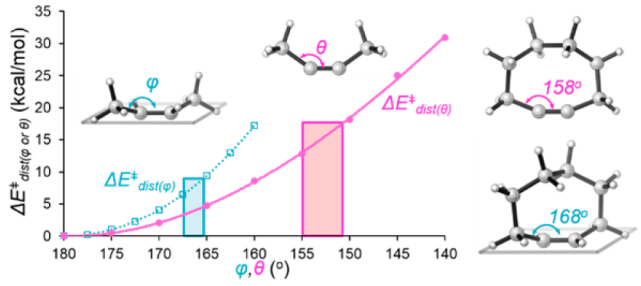

Figure 10. Left: plot of angular distortion energy ($\Delta E^{\ddagger}_{dist(\varphi)}$ or $\Delta E^{\ddagger}_{dist(\theta)}$) versus distortion angle (φ or θ) for *trans*-2-butene (blue) and 2-butyne (pink). The blue and pink boxes show the angles in the Diels–Alder transition states for *trans*-2-butene and 2-butyne. Right: geometries of ground-state *trans*-cyclooctene and cyclooctyne.

structures, respectively, as highlighted in blue and pink boxes (Figure 10).

Bending of 2-butyne in this way is easier than bending of *trans*-2-butene, which is in agreement with our previous study of nucleophilic additions of LiH and MeLi to ethylene and acetylene.[26] However, in the tetrazine Diels–Alder reactions, 2-butyne is bent more than *trans*-2-butene in the transition states, resulting in a higher net distortion energy.

A distortion/interaction analysis was also carried out on reactions of strained dienophiles with tetrazines to understand more quantitatively their high reactivities as compared to unstrained acyclic alkenes and alkynes. The energy components for transition structures of reactions involving dienophiles **10** and **11** are graphically displayed for each tetrazine in Figure 9 on the right. In comparison with the plot on the left, it shows that the significant drop in distortion energies involving strained dienophiles contributes to the decrease in activation energies. Detailed analyses of the distortions and interactions for the dimethyltetrazine reactions are given in Figure 11.

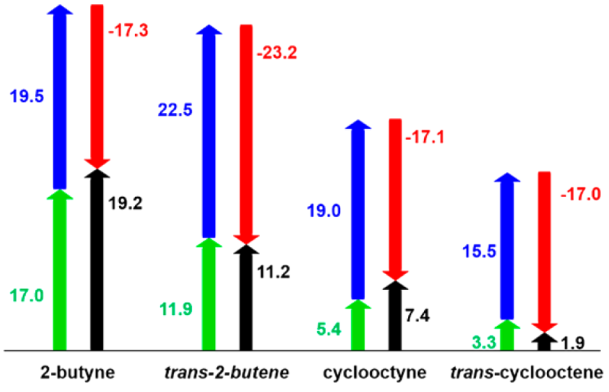

Figure 11. Graph of distortion, interaction, and activation energies for transition states of reactions between tetrazine **2** and dienophiles **8**–**11** (green: distortion energy of dienophile, blue: distortion energy of diene, red: interaction energy, black: activation energy, in kcal/mol).

Comparing the activation energies for 2-butyne and cyclooctyne, there is a 12 kcal/mol reduction in the activation energy, due to the predistortion of cyclooctyne.[7a,c] It takes little energy to distort the predistorted alkyne to the transition state. The same trend is observed upon comparison of *trans*-2-butene and *trans*-cyclooctene. Although the interaction energy is more negative for *trans*-2-butene due to a somewhat late TS (Figure 6), the extremely small distortion energy for *trans*-cyclooctene lowers the activation energy. The decrease in activation barriers results from the decrease in distortion energies of dienophiles. The distortion angles (φ and θ) in ground-state structures of *trans*-cyclooctene and cyclooctyne are 168° and 158°, respectively, as shown in Figure 10 on the right. These values are fairly close to the angles observed in transition structures, where φ ranges from 166° to 163°, and θ ranges from 154° to 149°. On the basis of this analysis, we conclude that compared to unstrained dienophiles, *trans*-cyclooctene and cyclooctyne are predistorted toward Diels–Alder transition structures and require much smaller distortion energies, leading to lower activation barriers.

Tetrazine Substituent Effect on the Diels–Alder Reactivity. The transition structures for the Diels–Alder reactions between tetrazines **1**–**7** and dienophile **9** are shown in Figure 12, and the forming C–C bond distances are marked in angstroms. The activation enthalpy ($\Delta H^{\ddagger}$), activation free energy ($\Delta G^{\ddagger}$), and reaction free energy (ΔG_{rxn}) are shown below each structure in kcal/mol in blue, red, and black, respectively.

Computational results reproduce the reactivity trends observed experimentally (Scheme 3). Dimethoxytetrazine **1** has the highest barrier and latest transition state with the shortest forming bond distances. Dimethyltetrazine **2** and diphenyltetrazine **3** have barriers slightly lower than that of **1** but are less reactive than parent tetrazine **4**. The reactivity of dipyridyltetrazine **5** is between that of parent tetrazine **4** and those of dimethyl tetrazine-3,6-dicarboxylate **6** and bis-(trifluoromethyl)tetrazine **7**.

To understand these reactivity patterns, we performed distortion/interaction analyses on these transition structures, as shown in Figure 13. The distortion energy of dienophile (green arrow), distortion energy of diene (blue arrow), interaction energy (red arrow), and activation energy (black arrow) are plotted for each tetrazine involved in the reaction. The distortion energy of dienophiles is not very sensitive to the tetrazine substituents, ranging only from 10 to 13 kcal/mol as the substituent varies. Distortion energies of *trans*-2-butene are higher for reactions involving donor-substituted tetrazines than for reactions involving acceptor-substituted tetrazines; this is due to the position of transition states. The tetrazine distortion energies vary from 19 to 25 kcal/mol. The distortion energies are larger for R = donor, where the transition states are relatively late, and become smaller for R = acceptor, where the transition states are relatively early. This difference in distortion energies is not as significant as the difference in interaction energies, which is the major contributor to the variance in activation energies. These vary from −20 to −33 kcal/mol. Tetrazines substituted with electron-withdrawing groups tend to have more negative interaction energies, leading to lower activation energies. This arises in large part from the favorable tetrazine LUMO+1 interaction with alkene HOMO, as discussed earlier.

To provide a more detailed understanding of how the distortion and interaction energies vary as the reaction proceeds, we have examined distortion and interaction energies along the intrinsic reaction coordinates (IRCs) for these reactions. The activation energies and energy components are plotted against the forming C–C bond distance for points along the IRCs in Figure 14a. This type of analysis has been used extensively by Bickelhaupt[24a,25a,b,e,f,l] and in our earlier work.[27] Activation, distortion, and interaction energies are shown as solid lines, dashed-dotted lines, and dashed lines,

dx.doi.org/10.1021/ja505569a | J. Am. Chem. Soc. 2014, 136, 11483–11493

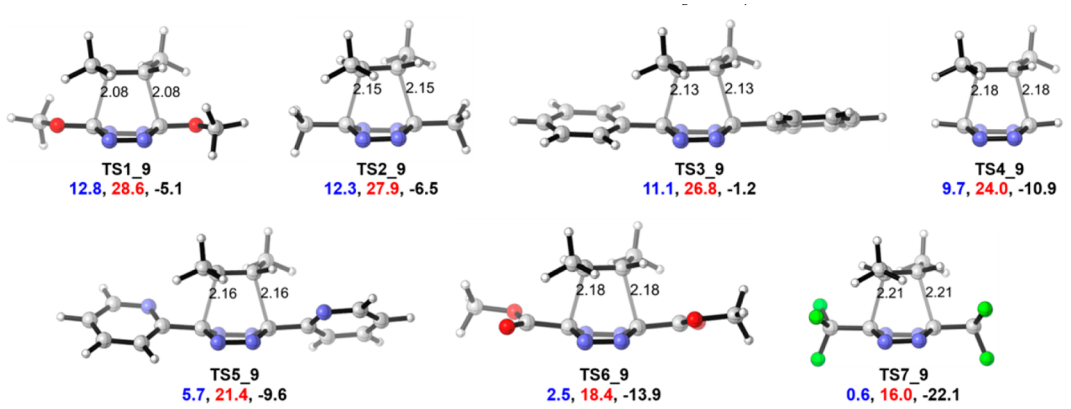

Figure 12. M06-2*X*/6-31G(d)-optimized transition structures for reactions of *trans*-2-butene with tetrazines (forming C−C bond distances are labeled in angstroms; $\Delta H^{\ddagger}$, $\Delta G^{\ddagger}$, and ΔG_{rxn} are shown below each structure in kcal/mol in blue, red, and black, respectively).

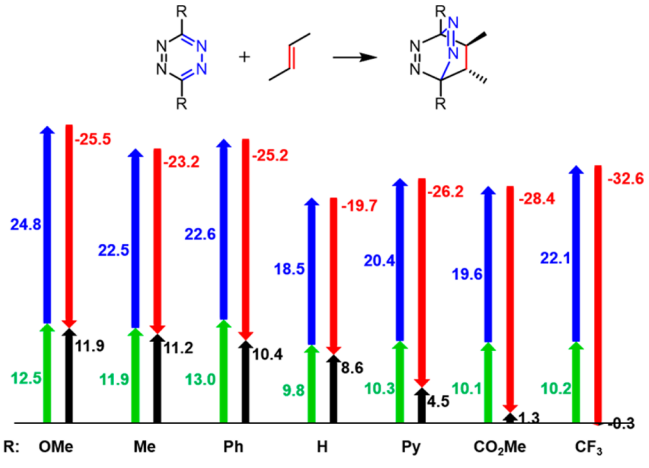

Figure 13. Graph of distortion, interaction, and activation energies for transition states of reactions between tetrazines **1**−**7** and *trans*-2-butene **9** (green: distortion energy of dienophile, blue: distortion energy of diene, red: interaction energy, black: activation energy, in kcal/mol).

respectively. These energy profiles are colored according to the tetrazines involved in the reactions. The positions of transition states are marked with diamonds in corresponding colors. The energy values at these positions correspond to the activation energy ($\Delta E^{\ddagger}_{act}$), total distortion energy ($\Delta E^{\ddagger}_{dist}$), and interaction energy ($\Delta E^{\ddagger}_{int}$) defined in Figure 8. At the transition state, the derivative of the distortion energy is equal and opposite in sign to the derivative of the interaction energy. Clearly, an early transition state, with a relatively long forming C−C bond distance, corresponds to a low activation barrier, while a late transition state is accompanied by a high activation barrier.

At a given forming bond distance, reactions involving tetrazines substituted with electron-withdrawing groups have stronger interaction energies than reactions of tetrazines substituted with electron-donating groups (Figure 14a, dashed lines). These differences in interaction energies can be explained readily by FMO theory. The variation in LUMO+1 energies of tetrazines **1**−**7** in Figure 3 corresponds approximately with the vertical displacement of the dashed lines in Figure 14a. Tetrazines substituted with electron-withdrawing groups have lower LUMO+1 energies, leading to smaller HOMO−LUMO+1 gaps and stronger interaction energies. We were surprised to discover that a correlation between energies and the electron-withdrawing abilities of the substituents does not hold true for the distortion energies (Figure 14a, dashed-dotted lines). At a certain forming bond distance, the reaction of dimethoxytetrazine **1** has a much smaller distortion energy than the reaction of bis(trifluoromethyl)tetrazine **7**, while the reactions involving tetrazines **2**−**6** have very similar distortion energies. Does this suggest that dimethoxytetrazine **1** is easier to distort than bis(trifluoromethyl)tetrazine **7**? To answer this question, we analyzed four critical structures along the IRCs for reactions involving **1** and **7** (Figure 14b), including two transition structures (**TS1_9** and **TS7_9**) and two structures with nearly the same forming bond distances as in the transition state for the other tetrazine. We call these comparison structures **M1_9** and **M7_9**.

At a nearly identical forming bond distance, dihedral angle N(1)−C(2)−O(3)−N(4) of dimethoxytetrazine is significantly larger than dihedral angle N(1)−C(2)−C(3)−N(4) of bis(trifluoromethyl)tetrazine (155° versus 145° or 145° versus 139°, shown in Figure 14b on the right), indicating that dimethoxytetrazine is less bent out of planarity than bis(trifluoromethyl)tetrazine when interacting with *trans*-2-butene at a certain distance. This explains why the distortion energy curve for dimethoxytetrazine is lower than that for bis(trifluoromethyl)tetrazine, not because the former is easier to distort but because the former is distorted to a lesser degree.

To compare the ease of distortion in substituted tetrazines, a scan of the out-of-plane distortion (Figure 15), which is a prominent distortion in the transition state, was carried out. For each tetrazine, the out-of-plane dihedral angle ω, which is 0° for planar ground-state structures and 12−18° for transition structures, was gradually increased from 2.5° to 20.0° in intervals of 2.5°. The energy difference between optimized structure with fixed dihedral angles and the ground-state structure is defined as the angular distortion energy ($\Delta E^{\ddagger}_{dist\_\omega}$). Figure 15 shows the plots of $\Delta E^{\ddagger}_{dist\_\omega}$ versus the dihedral angle ω.

The distortion energy increases as this dihedral angle increases. At a certain angle within the transition zone (highlighted with an orange box in Figure 15 with ω = 12−18°), the distortion energies of tetrazines substituted with electron-withdrawing groups are significantly lower than those of tetrazines substituted with electron-donating groups. The acceptor-substituted tetrazines are easier to distort than the donor-substituted tetrazines. This occurs because donors stabilize electron-deficient tetrazines, while acceptors destabilize

dx.doi.org/10.1021/ja505569a | J. Am. Chem. Soc. 2014, 136, 11483−11493

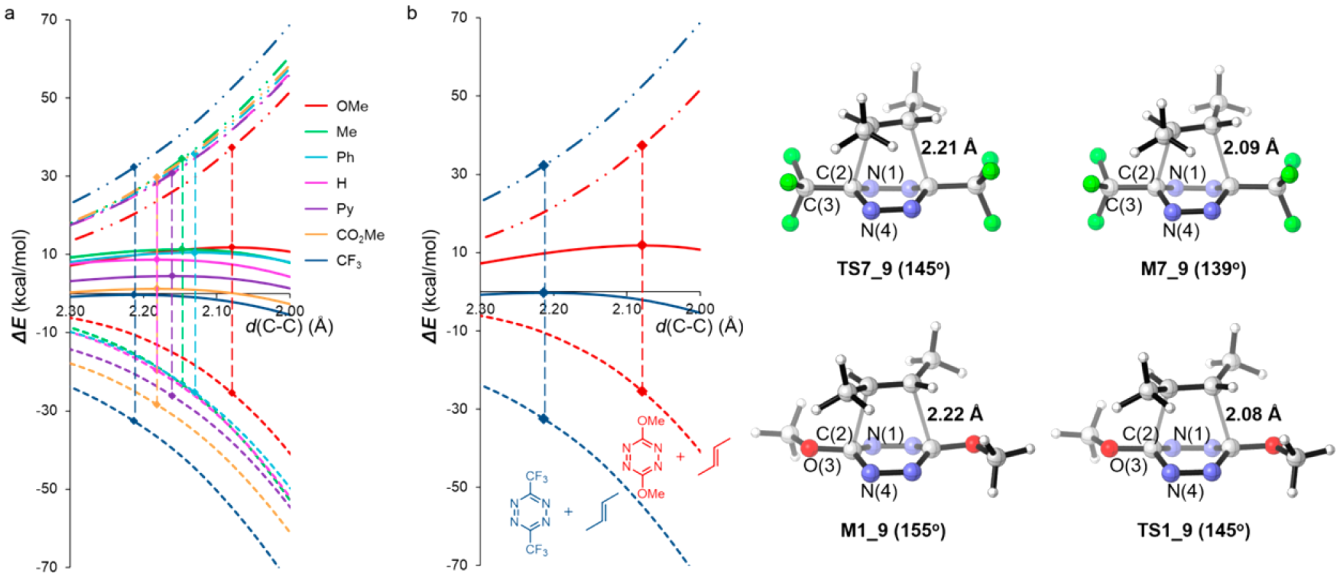

Figure 14. (a) Activation energy ΔE_{act} (solid), distortion energy ΔE_{dist} (dashed-dotted), and interaction energy ΔE_{int} (dashed) along the reaction coordinate (forming bond distance in angstroms) for reactions of tetrazines **1**–**7** with *trans*-2-butene **9**. (b) Left: Activation energy ΔE_{act} (solid), distortion energy ΔE_{dist} (dashed-dotted), and interaction energy ΔE_{int} (dashed) along the reaction coordinate (forming bond distance in angstroms) for reactions of tetrazines **1** (R = OMe, red) and **7** (R = CF_3, blue) with *trans*-2-butene. Right: transition structures for reactions of **1** and **7** with *trans*-2-butene (**TS1_9** and **TS7_9**) and structures of the corresponding IRC points with nearly the same forming bond distances as in the TS for the other tetrazine (**M1_9** and **M7_9**). The distortion angle N(1)–C(2)–C(3)–N(4) or N(1)–C(2)–O(3)–N(4) is shown below each structure.

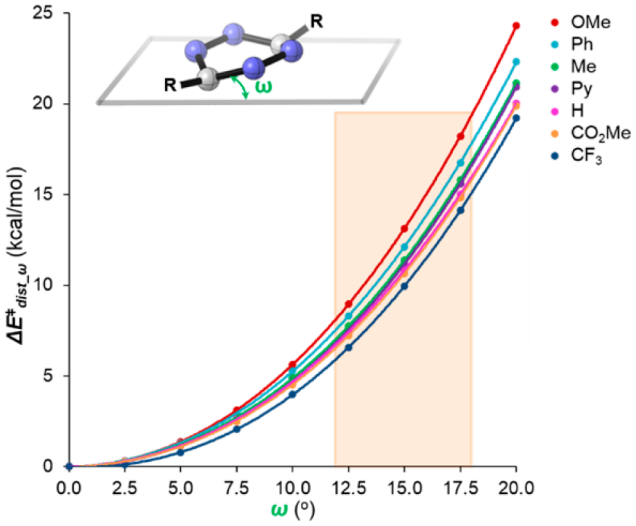

Figure 15. Plots of angular distortion energies ($\Delta E^{\ddagger}_{dist\_\omega}$) versus distortion angle (ω) for tetrazines **1**–**7**. The orange box shows the angles in the transition states for reactions of tetrazines **1**–**7** with dienophiles **8**–**11**.

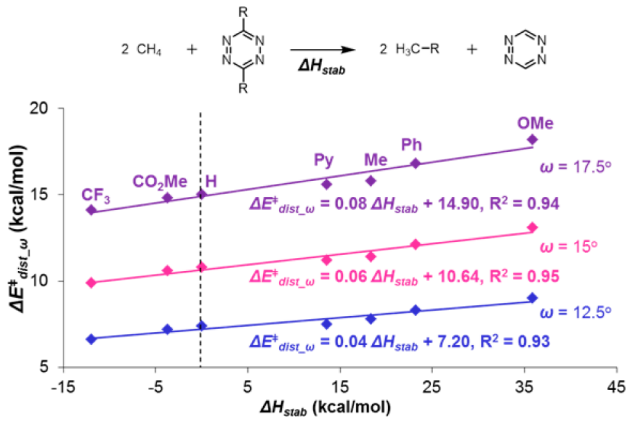

Figure 16. Correlation between angular distortion energies at fixed distortion angles (ω = 12.5°, 15.0°, and 17.5°) and the reaction enthalpies of the corresponding isodesmic reactions.

them. Tetrazine is electron-deficient, has low-energy vacant orbitals, and is stabilized by electron-donating substituents. This interaction is reduced by bending.

To evaluate the thermodynamic consequence of the interaction between substituents and the tetrazine nucleus, we calculated the isodesmic reaction energies for the process shown in Figure 16. The isodesmic reaction energy, ΔH_{stab}, is very favorable (35 kcal/mol stabilization energy) when the substituent is a strong donor (R = MeO), and it becomes unfavorable when the substituent becomes strong electron-withdrawing CF_3. The angular distortion energies at various values of ω are plotted versus ΔH_{stab} in Figure 16. The ease of distortion in substituted tetrazines is related to the stabilization of the ground-state structures by substituents. Tetrazines substituted by electron-donating groups are more stable and hard to distort, while tetrazines substituted by electron-withdrawing groups are less stable and easy to distort into the Diels–Alder transition-state geometries.

Finally, we summarize the factors that control reactivities of tetrazines. Figure 17 shows a plot of activation energies ($\Delta E^{\ddagger}_{act}$) versus total distortion energies ($\Delta E^{\ddagger}_{dist}$) and versus reaction energies ($\Delta E^{\ddagger}_{rxn}$). The blue and red data points on the plot are for the Diels–Alder reactions of tetrazines **1**–**7** with alkenes and alkynes, respectively. The solid and empty data points are for reactions involving strained and unstrained dienophiles, respectively. The linear correlations for all data are shown at the bottom right of each plot. As shown in Figure 17b, there is almost no correlation between the activation energies and reaction energies. As noted earlier, alkenes (blue), generally, are more reactive than alkynes (red), but the reaction

dx.doi.org/10.1021/ja505569a | J. Am. Chem. Soc. 2014, 136, 11483–11493

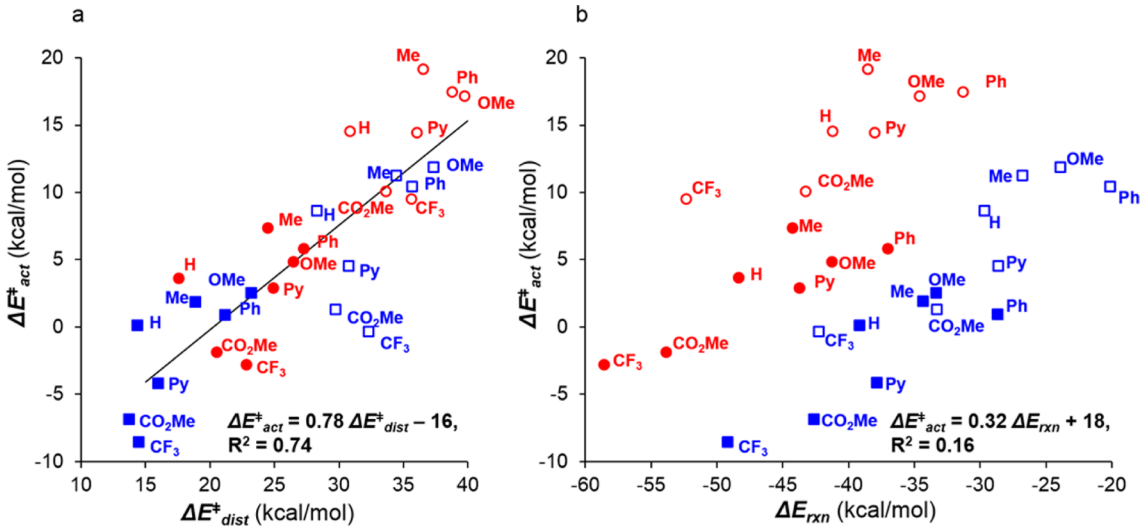

Figure 17. Plots of activation energy ($\Delta E^{\ddagger}_{act}$) versus (a) total distortion energy ($\Delta E^{\ddagger}_{dist}$) and (b) reaction energy (ΔE_{rxn}). Solid blue squares: *trans*-cyclooctene; empty blue squares: *trans*-2-butene; solid red circles: cyclooctyne; empty red circles: 2-butyne. The labels shown beside each data point refer to the substituents of the tetrazines.

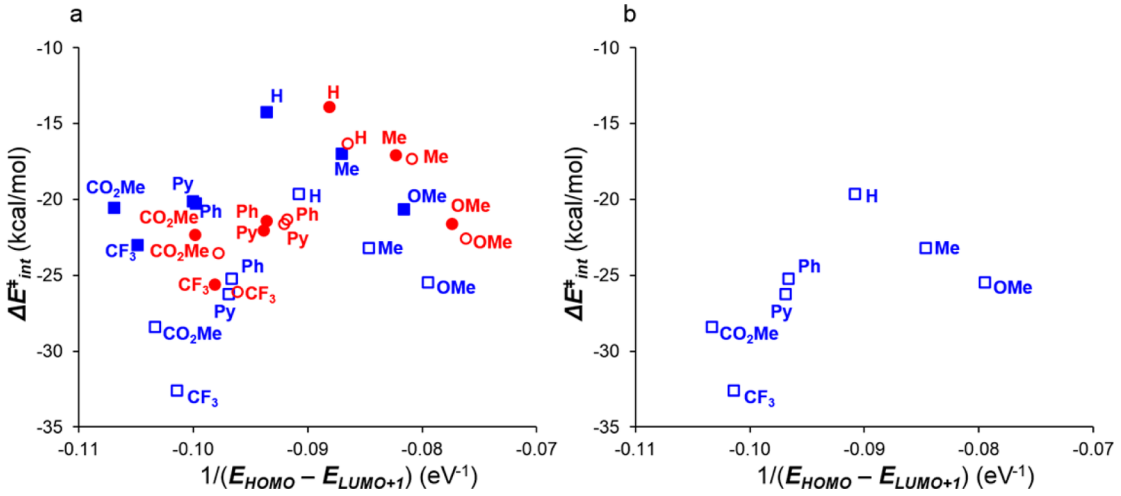

Figure 18. (a) Plots of interaction energy ($\Delta E^{\ddagger}_{int}$) versus inverse of the FMO energy gap ($1/(E_{HOMO} - E_{LUMO+1})$). Solid blue squares: *trans*-cyclooctene; empty blue squares: *trans*-2-butene; solid red circles: cyclooctyne; empty red circles: 2-butyne. The labels shown beside each data point refer to the substituents of the tetrazines. (b) Same plot for *trans*-2-butene only.

energies with alkenes are much less exothermic than those with alkynes. This shows up quite dramatically in Figure 17b, where the blue alkene points are all below and on the right of the corresponding red alkyne points.

The correlation between activation energy and distortion energy is much better, with R^2 equal to 0.74. The activation energies increase as the distortion energies increase. In general, this correlation indicates that the reactivity is mainly controlled by distortion. Deviations from this line result from the fact that interaction energies are not constant. Tetrazines with electron-donating substituents generally lie at or above the correlation line, while tetrazines with electron-withdrawing substituents mostly lie below this line, due to their more favorable interaction energies. The interaction energy differences cause deviations from the linear correlation with distortion energies.

Interaction energies arise from a variety of factors, such as charge-transfer, electrostatic, and polarization stabilization, as well as closed-shell (Pauli) repulsion. The differences in interaction energies are largely determined by differences in charge-transfer stabilization due to dienophile HOMO and tetrazine LUMO+1 interaction in the reaction studied here. According to perturbation theory, the stabilization energy arising from this interaction is proportional to $1/(E_{HOMO} - E_{LUMO+1})$.[28] On the basis of this, we expect a larger interaction energy for the tetrazines substituted by electron-withdrawing groups. This is only qualitatively the case, as shown by the plot of $\Delta E^{\ddagger}_{int}$ versus $1/(E_{HOMO} - E_{LUMO+1})$ in Figure 18. The significant deviations arise from the complication that the interaction energies are altered by the position of transition states.

For each type of dienophile, a "volcano" type correlation is observed. Figure 18b shows this for *trans*-2-butene. The largest stabilizing interaction energies are at the lower left of the graph, involving a very low-energy tetrazine LUMO+1; moving to the right of the graph, poorer acceptors have increasing LUMO+1 energies, and the HOMO−LUMO+1 gap increases, resulting in less favorable interaction energy. The methyl and methoxy compounds have higher LUMO+1 energies (Figure 3), and

dx.doi.org/10.1021/ja505569a | J. Am. Chem. Soc. 2014, 136, 11483−11493

larger HOMO−LUMO+1 gaps, but nevertheless more negative interaction energies due to their later transition states (Figure 14). This leads to the deviation of data points for R = OMe and Me from the linear correlations.

CONCLUSION

We have studied dienophile strain and tetrazine substituent effects on rates of Diels−Alder reactions of tetrazines. Electron-withdrawing substituents on tetrazines lower the LUMO+1 energy, leading to stronger interaction energies in Diels−Alder reactions with dienophiles, and simultaneously facilitate the crucial out-of-plane distortion that controls distortion energies. Small distortion energies and strong interaction energies explain the high reactivities of tetrazines substituted by electron-withdrawing groups. Electron-donating substituents affect reactivities in the opposite fashion. We have demonstrated that alkenes are in general more reactive than alkynes in Diels−Alder reactions with tetrazines. Alkenes have HOMO energies that are higher than those of alkynes, and therefore, alkenes have stronger interaction energies with electrophilic tetrazines. In addition, the distortion energies required for alkenes to achieve their transition structures are less than those for alkynes. Strained dienophiles are extremely reactive in the tetrazine cycloadditions because they are predistorted toward the transition structures. Consequently, much smaller distortion energies are required to achieve the transition-state geometries. The broad range of reactivities exhibited in the inverse-electron-demand Diels−Alder reactions of tetrazines can be tuned by tetrazine substituents and dienophile strain. The understanding of how distortion and interaction energies influence reactivity provides a guide to future developments of these reactions for uses in many areas of chemistry and biology.

ASSOCIATED CONTENT

Supporting Information

Computational details. This material is available free of charge via the Internet at http://pubs.acs.org.

AUTHOR INFORMATION

Corresponding Author

houk@chem.ucla.edu

Notes

The authors declare no competing financial interest.

ACKNOWLEDGMENTS

We are grateful to the National Science Foundation (CHE-1059084) for financial support of this research. Calculations were performed on the Hoffman2 cluster at UCLA and the Extreme Science and Engineering Discovery Environment (XSEDE), which is supported by the NSF (OCI-1053575).

REFERENCES

(1) For reviews, see: (a) Devaraj, N. K.; Weissleder, R. *Acc. Chem. Res.* **2011**, *44*, 816. (b) Schmidt, M. J.; Summerer, D. *ChemBioChem* **2012**, *13*, 1553. (c) Knall, A.-C.; Slugovc, C. *Chem. Soc. Rev.* **2013**, *42*, 5131. (d) Carroll, L.; Evans, H. L.; Aboagye, E. O.; Spivey, A. C. *Org. Biomol. Chem.* **2013**, *11*, 5772. (e) Debets, M. F.; van Hest, J. C. M.; Rutjes, F. P. J. T. *Org. Biomol. Chem.* **2013**, *11*, 6439. (f) Lang, K.; Chin, J. W. *ACS Chem. Biol.* **2014**, *9*, 16. (g) Patterson, D. M.; Nazarova, L. A.; Prescher, J. A. *ACS Chem. Biol.* **2014**, *9*, 592.

(2) (a) Blackman, M. L.; Royzen, M.; Fox, J. M. *J. Am. Chem. Soc.* **2008**, *130*, 13518. (b) Devaraj, N. K.; Weissleder, R.; Hilderbrand, S. A. *Bioconjugate Chem.* **2008**, *19*, 2297.

(3) (a) Devaraj, N. K.; Upadhyay, R.; Haun, J. B.; Hilderbrand, S. A.; Weissleder, R. *Angew. Chem., Int. Ed.* **2009**, *48*, 7013. (b) Devaraj, N. K.; Hilderbrand, S.; Upadhyay, R.; Mazitschek, R.; Weissleder, R. *Angew. Chem., Int. Ed.* **2010**, *49*, 2869. (c) Budin, G.; Yang, K. S.; Reiner, T.; Weissleder, R. *Angew. Chem., Int. Ed.* **2011**, *50*, 9378. (d) Yang, K. S.; Budin, G.; Reiner, T.; Vinegoni, C.; Weissleder, R. *Angew. Chem., Int. Ed.* **2012**, *51*, 6598. (e) Devaraj, N. K.; Thurber, G. M.; Keliher, E. J.; Marinelli, B.; Weissleder, R. *Proc. Natl. Acad. Sci. U. S. A.* **2012**, *109*, 4762. (f) Liu, D. S.; Tangpeerachaikul, A.; Selvaraj, R.; Taylor, M. T.; Fox, J. M.; Ting, A. Y. *J. Am. Chem. Soc.* **2012**, *134*, 792. (g) Carlson, J. C. T.; Meimetis, L. G.; Hilderbrand, S. A.; Weissleder, R. *Angew. Chem., Int. Ed.* **2013**, *52*, 6917. (h) Lukinavicius, G.; Umezawa, K.; Olivier, N.; Honigmann, A.; Yang, G.; Plass, T.; Mueller, V.; Reymond, L.; Corrêa, I. R., Jr.; Luo, Z.-G.; Schultz, C.; Lemke, E. A.; Heppenstall, P.; Eggeling, C.; Manley, S.; Johnsson, K. *Nat. Chem.* **2013**, *5*, 132. (i) Nikic, I.; Plass, T.; Schraidt, O.; Szymanski, J.; Briggs, J. A. G.; Schultz, C.; Lemke, E. A. *Angew. Chem., Int. Ed.* **2014**, *53*, 2245. (j) Wu, H.; Yang, J.; Šečkutė, J.; Devaraj, N. K. *Angew. Chem., Int. Ed.* **2014**, *53*, 5805. (k) Denk, C.; Svatunek, D.; Filip, T.; Wanek, T.; Lumpi, D.; Frohlich, J.; Kuntner, C.; Mikula, H. *Angew. Chem., Int. Ed.* **2014**, *53*, DOI: 10.1002/anie.201404277.

(4) (a) Yang, J.; Šečkutė, J.; Cole, C. M.; Devaraj, N. K. *Angew. Chem., Int. Ed.* **2012**, *51*, 7476. (b) Patterson, D. M.; Nazarova, L. A.; Xie, B.; Kamber, D. N.; Prescher, J. A. *J. Am. Chem. Soc.* **2012**, *134*, 18638. (c) Kamber, D. N.; Nazarova, L. A.; Liang, Y.; Lopez, S. A.; Patterson, D. M.; Shih, H.-W.; Houk, K. N.; Prescher, J. A. *J. Am. Chem. Soc.* **2013**, *135*, 13680. (d) Cole, C. M.; Yang, J.; Šečkutė, J.; Devaraj, N. K. *ChemBioChem.* **2013**, *14*, 205. (e) Šečkutė, J.; Yang, J.; Devaraj, N. K. *Nucleic Acids Res.* **2013**, *41*, e148. (f) Yang, J.; Liang, Y.; Šečkutė, J.; Houk, K. N.; Devaraj, N. K. *Chem.—Eur. J.* **2014**, *20*, 3365. (g) Patterson, D. M.; Jones, K. A.; Prescher, J. A. *Mol. Biosyst.* **2014**, *10*, 1693. (h) Sachdeva, A.; Wang, K.; Elliott, T.; Chin, J. W. *J. Am. Chem. Soc.* **2014**, *136*, 7785. (i) Li, Z.; Wang, D.; Li, L.; Pan, S.; Na, Z.; Tan, C. Y. J.; Yao, S. Q. *J. Am. Chem. Soc.* **2014**, *136*, 9990.

(5) (a) Pipkorn, R.; Waldeck, W.; Didinger, B.; Koch, M.; Mueller, G.; Wiessler, M.; Braun, K. *J. Pept. Sci.* **2009**, *15*, 235. (b) Engelsma, S. B.; Willems, L. I.; van Paaschen, C. E.; van Kasteren, S. I.; van der Marel, G. A.; Overkleeft, H. S.; Filippov, D. V. *Org. Lett.* **2014**, *16*, 2744.

(6) (a) Chen, W.; Wang, D.; Dai, C.; Hamelberg, D.; Wang, B. *Chem. Commun.* **2012**, *48*, 1736. (b) Plass, T.; Milles, S.; Koehler, C.; Szymanski, J.; Mueller, R.; Wiebler, M.; Schultz, C.; Lemke, E. A. *Angew. Chem., Int. Ed.* **2012**, *51*, 4166. (c) Thomas, J. D.; Cui, H.; North, P. J.; Hofer, T.; Rader, C.; Burke, T. R., Jr. *Bioconjugate Chem.* **2012**, *23*, 2007. (d) Lang, K.; Davis, L.; Wallace, S.; Mahesh, M.; Cox, D. J.; Blackman, M. L.; Fox, J. M.; Chin, J. W. *J. Am. Chem. Soc.* **2012**, *134*, 10317.

(7) (a) Schoenebeck, F.; Ess, D. H.; Jones, G. O.; Houk, K. N. *J. Am. Chem. Soc.* **2009**, *131*, 8121. (b) Paton, R. S.; Kim, S.; Ross, A. G.; Danishefsky, S. J.; Houk, K. N. *Angew. Chem., Int. Ed.* **2011**, *50*, 10366. (c) Gordon, C. G.; Mackey, J. L.; Jewett, J. C.; Sletten, E. M.; Houk, K. N.; Bertozzi, C. R. *J. Am. Chem. Soc.* **2012**, *134*, 9199. (d) Liang, Y.; Mackey, J. L.; Lopez, S. A.; Liu, F.; Houk, K. N. *J. Am. Chem. Soc.* **2012**, *134*, 17904. (e) Liu, F.; Paton, R. S.; Kim, S.; Liang, Y.; Houk, K. N. *J. Am. Chem. Soc.* **2013**, *135*, 15642.

(8) (a) Boger, D. L.; Wolkenberg, S. E. *J. Org. Chem.* **2000**, *65*, 9120. (b) Boger, D. L.; Hong, J. *J. Am. Chem. Soc.* **2001**, *123*, 8515. (c) Hamasaki, A.; Zimpleman, J. M.; Hwang, I.; Boger, D. L. *J. Am. Chem. Soc.* **2005**, *127*, 10767. (d) Oakdale, J. S.; Boger, D. L. *Org. Lett.* **2010**, *12*, 1132. (e) Fu, L.; Gribble, G. W. *Tetrahedron Lett.* **2010**, *51*, 537.

(9) Chen, C.; Allen, C. A.; Cohen, S. M. *Inorg. Chem.* **2011**, *50*, 10534.

(10) (a) Hayden, H.; Gun'ko, Y. K.; Perova, T. S. *Chem. Phys. Lett.* **2007**, *435*, 84. (b) Hayden, H.; Gun'ko, Y. K.; Perova, T.; Grudinkin, S.; Moore, A.; Obraztsova, E. D. *Plast. Rubber Compos.* **2009**, *38*, 253. (c) Zhu, J.; Hiltz, J.; Lennox, R. B.; Schirrmacher, R. *Chem. Commun.* **2013**, *49*, 10275.

(11) (a) Beckmann, H. S. G.; Niederwieser, A.; Wiessler, M.; Wittmann, V. *Chem.—Eur. J.* **2012**, *18*, 6548. (b) Zhang, C.-J.; Tan, C. Y. J.; Ge, J.; Na, Z.; Chen, G. Y. J.; Uttamchandani, M.; Sun, H.; Yao, S. Q. *Angew. Chem., Int. Ed.* **2013**, *52*, 14060.
(12) (a) Sauer, J.; Mielert, A.; Lang, D.; Peter, D. *Chem. Ber.* **1965**, *98*, 1435. (b) Sauer, J.; Heinrichs, G. *Tetrahedron Lett.* **1966**, *41*, 4979. (c) Thalhammer, F.; Wallfahrer, U.; Sauer, J. *Tetrahedron Lett.* **1990**, *31*, 6851. (d) Meier, A.; Sauer, J. *Tetrahedron Lett.* **1990**, *31*, 6855. (e) Cioslowski, J.; Sauer, J.; Hetzenegger, J.; Karcher, T.; Hierstetter, T. *J. Am. Chem. Soc.* **1993**, *115*, 1353. (f) Sauer, J.; Heldmann, D. K.; Hetzenegger, J.; Krauthan, J.; Sichert, H.; Schuster, J. *Eur. J. Org. Chem.* **1998**, 2885. (g) Sauer, J.; Bäuerlein, P.; Ebenbeck, W.; Gousetis, C.; Sichert, H.; Troll, T.; Utz, F.; Wallfahrer, U. *Eur. J. Org. Chem.* **2001**, 2629.
(13) (a) Carboni, R. A.; Lindsey, R. V., Jr. *J. Am. Chem. Soc.* **1959**, *81*, 4342. (b) Boger, D. L.; Panek, J. S. *J. Am. Chem. Soc.* **1985**, *107*, 5745. (c) Sakya, S.; Groskopf, K. K.; Boger, D. L. *Tetrahedron Lett.* **1997**, *38*, 3805. (d) Boger, D. L.; Boyce, C. W.; Labroli, M. A.; Sehon, C. A.; Jin, Q. *J. Am. Chem. Soc.* **1999**, *121*, 54.
(14) Bach, R. D. *J. Am. Chem. Soc.* **2009**, *131*, 5233.
(15) Karver, M. R.; Weissleder, R.; Hilderbrand, S. A. *Bioconjugate Chem.* **2011**, *22*, 2263.
(16) Frisch, M. J.; Trucks, G. W.; Schlegel, H. B.; Scuseria, G. E.; Robb, M. A.; Cheeseman, J. R.; Scalmani, G.; Barone, V.; Mennucci, B.; Petersson, G. A.; Nakatsuji, H.; Caricato, M.; Li, X.; Hratchian, H. P.; Izmaylov, A. F.; Bloino, J.; Zheng, G.; Sonnenberg, J. L.; Hada, M.; Ehara, M.; Toyota, K.; Fukuda, R.; Hasegawa, J.; Ishida, M.; Nakajima, T.; Honda, Y.; Kitao, O.; Nakai, H.; Vreven, T.; Montgomery, J. A., Jr.; Peralta, J. E.; Ogliaro, F.; Bearpark, M.; Heyd, J. J.; Brothers, E.; Kudin, K. N.; Staroverov, V. N.; Keith, T.; Kobayashi, R.; Normand, J.; Raghavachari, K.; Rendell, A.; Burant, J. C.; Iyengar, S. S.; Tomasi, J.; Cossi, M.; Rega, N.; Millam, J. M.; Klene, M.; Knox, J. E.; Cross, J. B.; Bakken, V.; Adamo, C.; Jaramillo, J.; Gomperts, R.; Stratmann, R. E.; Yazyev, O.; Austin, A. J.; Cammi, R.; Pomelli, C.; Ochterski, J. W.; Martin, R. L.; Morokuma, K.; Zakrzewski, V. G.; Voth, G. A.; Salvador, P.; Dannenberg, J. J.; Dapprich, S.; Daniels, A. D.; Farkas, O.; Foresman, J. B.; Ortiz, J. V.; Cioslowski, J.; Fox, D. J. *Gaussian 09, revision D.01*; Gaussian Inc., Wallingford, CT, 2013.
(17) (a) Zhao, Y.; Truhlar, D. G. *Theor. Chem. Acc.* **2008**, *120*, 215. (b) Zhao, Y.; Truhlar, D. G. *Acc. Chem. Res.* **2008**, *41*, 157.
(18) (a) Zhao, Y.; Truhlar, D. G. *Phys. Chem. Chem. Phys.* **2008**, *10*, 2813. (b) Ribeiro, R. F.; Marenich, A. V.; Cramer, C. J.; Truhlar, D. G. *J. Phys. Chem. B* **2011**, *115*, 14556.
(19) (a) Paton, R. S.; Mackey, J. L.; Kim, W. H.; Lee, J. H.; Danishefsky, S. J.; Houk, K. N. *J. Am. Chem. Soc.* **2010**, *132*, 9335. (b) Lan, Y.; Zou, L.-F.; Cao, Y.; Houk, K. N. *J. Phys. Chem. A* **2011**, *115*, 13906.
(20) (a) Barone, V.; Cossi, M. *J. Phys. Chem. A* **1998**, *102*, 1995. (b) Cossi, M.; Rega, N.; Scalmani, G.; Barone, V. *J. Comput. Chem.* **2003**, *24*, 669. (c) Takano, Y.; Houk, K. N. *J. Chem. Theory Comput.* **2005**, *1*, 70.
(21) (a) Politzer, P.; Abu-Awwad, F. *Theor. Chem. Acc.* **1998**, *99*, 83. (b) Kar, T.; Angyan, J. G.; Sannigrahi, A. B. *J. Phys. Chem. A* **2000**, *104*, 9953. (c) Zhang, G.; Musgrave, C. B. *J. Phys. Chem. A* **2007**, *111*, 1554.
(22) The second-order rate constants measured experimentally by Sauer et al. (see ref 12c) for the cycloaddition reactions of dimethyl 1,2,4,5-tetrazine-3,6-dicarboxylate (**6**) with *trans*-4-octene and *cis*-4-octene are 0.0033 and 0.00048 M^{-1} s^{-1}, respectively. Calculations show that the activation free energy for the reaction of **6** with *cis*-2-butene is 0.3 kcal/mol higher than that with *trans*-2-butene. This suggests that *cis*-alkene is slightly less reactive than *trans*-alkene, in agreement with the experimental reactivity trend.
(23) (a) Ess, D. H.; Houk, K. N. *J. Am. Chem. Soc.* **2007**, *129*, 10646. (b) Ess, D. H.; Houk, K. N. *J. Am. Chem. Soc.* **2008**, *130*, 10187.
(24) For reviews, see: (a) van Zeist, W.-J.; Bickelhaupt, F. M. *Org. Biomol. Chem.* **2010**, *8*, 3118. (b) Fernández, I. *Phys. Chem. Chem. Phys.* **2014**, *16*, 7662.
(25) For recent examples, see: (a) Fernández, I.; Bickelhaupt, F. M. *J. Comput. Chem.* **2012**, *33*, 509. (b) Fernández, I.; Bickelhaupt, F. M.; Cossío, F. P. *Chem.—Eur. J.* **2012**, *18*, 12395. (c) Lopez, S. A.; Houk, K. N. *J. Org. Chem.* **2013**, *78*, 1778. (d) Zou, L.; Paton, R. S.; Eschenmoser, A.; Newhouse, T. R.; Baran, P. S.; Houk, K. N. *J. Org. Chem.* **2013**, *78*, 4037. (e) Fernández, I.; Bickelhaupt, F. M.; Uggerud, E. *J. Org. Chem.* **2013**, *78*, 8574. (f) Fernández, I.; Sola, M.; Bickelhaupt, F. M. *Chem.—Eur. J.* **2013**, *19*, 7416. (g) Usharani, D.; Lacy, D. C.; Borovik, A. S.; Shaik, S. *J. Am. Chem. Soc.* **2013**, *135*, 17090. (h) Morin, M. S. T.; St-Cyr, D. J.; Arndtsen, B. A.; Krenske, E. H.; Houk, K. N. *J. Am. Chem. Soc.* **2013**, *135*, 17349. (i) Hong, X.; Liang, Y.; Griffith, A. K.; Lambert, T. H.; Houk, K. N. *Chem. Sci.* **2014**, *5*, 471. (j) Yang, Y.-F.; Cheng, G.-J.; Liu, P.; Leow, D.; Sun, T.-Y.; Chen, P.; Zhang, X.; Yu, J.-Q.; Wu, Y.-D.; Houk, K. N. *J. Am. Chem. Soc.* **2014**, *136*, 344. (k) Hong, X.; Liang, Y.; Houk, K. N. *J. Am. Chem. Soc.* **2014**, *136*, 2017. (l) Fernández, I.; Bickelhaupt, F. M. *J. Comput. Chem.* **2014**, *35*, 371. (m) Liu, S.; Lei, Y.; Qi, X.; Lan, Y. *J. Phys. Chem. A* **2014**, *118*, 2638.
(26) (a) Strozier, R. W.; Caramella, P.; Houk, K. N. *J. Am. Chem. Soc.* **1979**, *101*, 1340. (b) Houk, K. N.; Rondan, N. G.; Schleyer, P. v. R.; Kaufmann, E.; Clark, T. *J. Am. Chem. Soc.* **1985**, *107*, 2821.
(27) (a) Hayden, A. E.; Houk, K. N. *J. Am. Chem. Soc.* **2009**, *131*, 4084. (b) Lan, Y.; Wheeler, S. E.; Houk, K. N. *J. Chem. Theory Comput.* **2011**, *7*, 2104.
(28) Houk, K. N. *Acc. Chem. Res.* **1975**, *8*, 361.